Neuron
Article

Dopaminergic Modulation of Axon Initial Segment Calcium Channels Regulates Action Potential Initiation

Kevin J. Bender,[1,2,*] Christopher P. Ford,[2] and Laurence O. Trussell[1,2]
[1]Oregon Hearing Research Center
[2]Vollum Institute
Oregon Health and Science University, Portland, OR 97239, USA
*Correspondence: benderke@ohsu.edu
DOI 10.1016/j.neuron.2010.09.026

SUMMARY

Action potentials initiate in the axon initial segment (AIS), a specialized compartment enriched with Na^+ and K^+ channels. Recently, we found that T- and R-type Ca^{2+} channels are concentrated in the AIS, where they contribute to local subthreshold membrane depolarization and thereby influence action potential initiation. While periods of high-frequency activity can alter availability of AIS voltage-gated channels, mechanisms for long-term modulation of AIS channel function remain unknown. Here, we examined the regulatory pathways that control AIS Ca^{2+} channel activity in brainstem interneurons. T-type Ca^{2+} channels were downregulated by dopamine receptor activation acting via protein kinase C, which in turn reduced neuronal output. These effects occurred without altering AIS Na^+ or somatodendritic T-type channel activity and could be mediated by endogenous dopamine sources present in the auditory brainstem. This pathway represents a new mechanism to inhibit neurons by specifically regulating Ca^{2+} channels directly involved in action potential initiation.

INTRODUCTION

The axon initial segment (AIS) has the lowest threshold for action potential (AP) initiation due to its high Na^+ channel density (Kole and Stuart, 2008), and it is therefore the site of AP initiation in most neurons (Coombs et al., 1957; Khaliq and Raman, 2006; Kress et al., 2008; Martina et al., 2000; Palmer and Stuart, 2006; Schmidt-Hieber et al., 2008; Shu et al., 2007; Stuart et al., 1997). Classically, the AIS was thought to be enriched only in Na^+ and K^+ channels (Bean, 2007; Kress and Mennerick, 2009). Using Ca^{2+} imaging, we recently discovered that the AIS may also contain T-type (Ca_V3) and R-type ($Ca_V2.3$) Ca^{2+} channels. AIS Ca^{2+} transients have been observed with Ca^{2+}-sensitive dyes in a variety of neuronal classes, including brainstem interneurons, cortical pyramidal neurons, and cerebellar Purkinje neurons (Bender and Trussell, 2009; Callewaert et al., 1996; Lüscher et al., 1996; Schiller et al., 1995), indicating that AIS Ca^{2+} channels may be a common feature of many neuronal classes. In concert with subthreshold Na^+ channel activation, AIS Ca^{2+} channels contribute to local subthreshold membrane depolarization and therefore determine if and when an excitatory synaptic input evokes an AP (Bender and Trussell, 2009).

The biophysical properties of voltage-gated channels in the AIS control AP initiation. Availability of Na^+ and K^+ channels depends on recent activity or membrane potential, leading to corresponding alterations in AP waveforms and threshold (Azouz and Gray, 2000; Goldberg et al., 2008; Hu et al., 2009; Kole et al., 2007). T-type Ca^{2+} channels, which are thought to contribute to the generation of AP bursts, inactivate as a neuron depolarizes, altering neuronal firing patterns (Kim and Trussell, 2007; Uebachs et al., 2006). These changes occur on the time scale of seconds; however, it remains unknown what mechanisms exist for long-term control of AIS excitability through second-messenger-dependent modification of constituent channels.

Here, we examined regulatory mechanisms that control the excitability of dorsal cochlear nucleus (DCN) cartwheel interneurons. Cartwheel cells are ideal for studying mechanisms of AP initiation because they intrinsically fire APs in a variety of ways, including bursts and single spikes, and the underlying ion channels that determine AP output in both the somatodendritic compartment and the AIS are relatively well understood (Bender and Trussell, 2009; Kim and Trussell, 2007). In these cells, we found that dopamine altered neuronal output by modification of T-type Ca^{2+} channels involved in AP initiation. Dopamine receptor activation, either by exogenous or endogenous agonists, activated protein kinase C (PKC), leading to inhibition of AIS T-type channels. This pathway was specific for AIS T-type channels; dopamine receptor activation had no effect on intrinsic cell properties, somatodendritic T-type Ca^{2+} channels, AIS Na^+ influx, or whole-cell K^+ and persistent Na^+ currents. Similar to direct antagonist block of AIS Ca^{2+} channels (Bender and Trussell, 2009), activation of this pathway ultimately reduced the AP output of these auditory interneurons. Thus, these data are the first direct evidence of ion channel modulation in the AIS and suggest that dopaminergic signaling mediates fine-scale adjustments of neuronal output by controlling the activity of AIS Ca^{2+} channels.

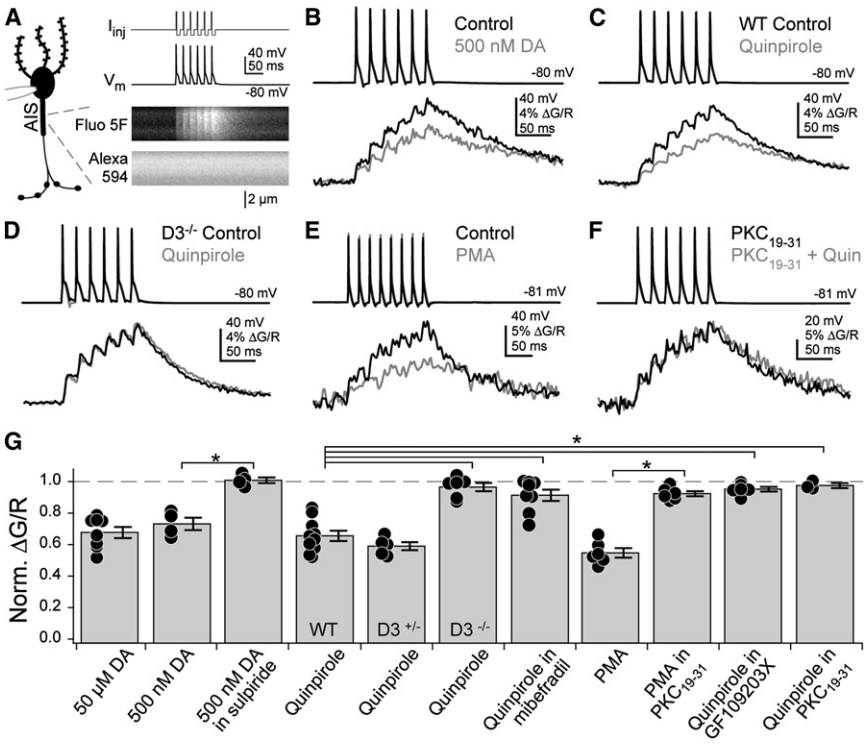

Figure 1. Dopamine Reduces AIS Ca^{2+} Transients in Cartwheel Cells

(A) Left: schematic of recording/imaging configuration. Whole-cell recordings were made from cartwheel cell somata, and Ca^{2+} transients were imaged in the AIS. Top right: AP trains were evoked by somatic current injection followed by negative current steps to ensure that only 1 AP was evoked per step. Bottom right: corresponding Fluo-5F (Ca^{2+}) and Alexa 594 (morphology) signals in AIS.

(B–F) AP train-evoked Ca^{2+} influx in the AIS. Shades correspond to drug conditions to right of AP trains. All Ca^{2+} transients were computed as the change in green fluorescence (G, Fluo-5F) over red fluorescence (R, Alexa). DA: dopamine. WT: wild-type.

(G) Summary of pharmacological effects on AIS Ca^{2+}. Values normalized to baseline ΔG/R amplitudes. For conditions expressed as "Drug X in Drug Y," normalized ΔG/R amplitudes reflect any changes mediated by Drug X relative to a baseline period in Drug Y. Dots are single cells. Error bars are SEM. Asterisk: $p < 0.0001$.

RESULTS

Axon Initial Segment Ca^{2+} Channels Are Regulated by Dopamine

Whole-cell recordings were made from DCN cartwheel cells in acute brain slices prepared from 16- to 24-day-old mice. Cells were filled via patch pipettes with the red volume marker Alexa 594 and the green Ca^{2+}-sensitive fluorophore Fluo-5F. Morphology and Ca^{2+} activity were visualized with a two-photon microscope. To examine AIS Ca^{2+} channel modulation, we evoked AP trains with somatic current injection and imaged concomitant Ca^{2+} transients 14–18 µm from the axon hillock (Figure 1A). Using these techniques, we showed previously that Ca^{2+} transients imaged at these locations were blocked by the T- and R-type Ca^{2+} channel antagonists mibefradil and SNX-482 (Bender and Trussell, 2009). AIS Ca^{2+} transients were also reduced by 50 µM Ni^{2+}, suggesting that the AIS contains the Ni^{2+}-sensitive $Ca_V3.2$ T-channel subunit (Lee et al., 1999). These channels are common targets for modulation via dopaminergic pathways (Chemin et al., 2006; Perez-Reyes, 2003) and indeed we found that dopamine, applied at a concentration of 500 nM or 50 µM, decreased AIS Ca^{2+} transients by 27% ± 4% (n = 4) and 32% ± 4% (n = 8), respectively (Figures 1B and 1G).

Dopamine can act through a variety of receptors, broadly grouped into dopamine receptor type 1 (D_1R and D_5R) and type 2 families (D_2R, D_3R, and D_4R). Dopamine-mediated effects on AIS Ca^{2+} transients were blocked by the D2-family specific antagonist sulpiride (Figure 1G; 200 nM, normalized ΔG/R: 1.01 ± 0.02, n = 4, $p < 0.0001$) and mimicked by the D_2-family agonist quinpirole (Figures 1C and 1G; 1 µM, normalized ΔG/R: 0.66 ± 0.03, n = 10), suggesting that AIS Ca^{2+} channels were regulated by D_2, D_3, or D_4 receptors. In situ hybridization labeling for D2-family mRNA shows D_3R mRNA in the DCN, but not D_2R or D_4R mRNA (Bouthenet et al., 1991; Heintz, 2004; Lein et al., 2007). Consistent with these results, quinpirole did not reduce AIS Ca^{2+} transients in D_3R knockout mice (Figures 1D and 1G; normalized ΔG/R: 0.96 ± 0.03, n = 6 cells, 3 animals, $p < 0.001$ versus wild-type). D_3R heterozygotes displayed a wild-type phenotype (normalized ΔG/R: 0.59 ± 0.03, n = 5, p = 0.2 versus wild-type).

Cartwheel cells express both T- and R-type Ca^{2+} channels in the AIS. These channels can be blocked by mibefradil, which acts on T- and R-type channels, and SNX-482, which acts on R-type channels. We observed previously that SNX-482-sensitive AIS Ca^{2+} transients persist in the presence of mibefradil, suggesting that mibefradil largely blocks T-type channels in the AIS (Bender and Trussell, 2009). Therefore, to determine whether T- or R-type channels were modulated by dopamine, we isolated AIS Ca^{2+} influx through R-type channels by imaging in the presence of 3 µM mibefradil. Consistent with previous results, AIS Ca^{2+} transients were 50.2% smaller in mibefradil compared to Ca^{2+} transients imaged in other cells in control conditions (n = 8 in mibefradil, 28 control, $p < 0.0001$, unpaired t test). Quinpirole had a small effect on these Ca^{2+} transients (Figure 1G; normalized ΔG/R: 0.91 ± 0.04, $p < 0.0001$ versus quinpirole without mibefradil). This could be due to modulation of either R-type channels or a fraction of T-type channels that was not blocked by 3 µM mibefradil (McDonough and Bean, 1998). Overall, these results suggest that dopamine primarily affected T-type channels.

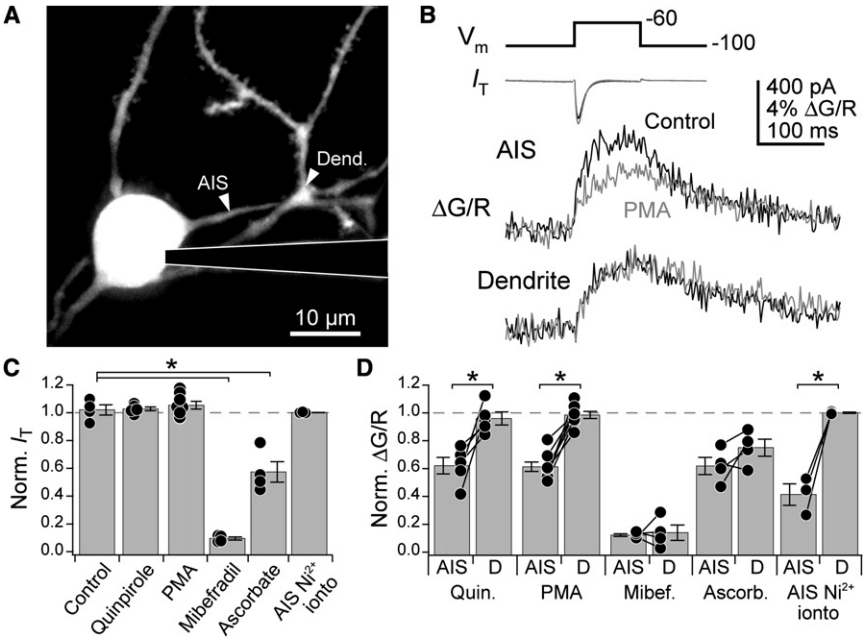

Figure 2. D_3R-PKC Pathway Is Specific for T-Type Channels Localized to the AIS

(A) Two-photon z stack of cartwheel cell. Arrowheads: sites of Ca^{2+} transients detailed in (B).

(B) Voltage steps from −100 to −60 mV evoked a whole-cell T current (I_T) and Ca^{2+} transients in the AIS and dendrite. Black: baseline, gray: in PMA.

(C and D) I_T (C) and normalized ΔG/R (D) following activation of D_3R-PKC pathway or block of T-type channels. Control currents were calculated as the relative I_T over a time course similar to that allowed for drug wash-in (12 min). Ni^{2+} was iontophoresed locally to the AIS. All other drugs were added to the recording solution. Dots are single cells. Lines connecting dots in (D) link recordings made in the same cell in the AIS and dendrite. Dendritic recordings are denoted with a "D." Bars are SEM. Asterisk: $p < 0.05$.

D_3R signaling may decrease AIS Ca^{2+} influx by activating protein kinase pathways that phosphorylate AIS T-type Ca^{2+} channels (Perez-Reyes, 2003; Ron et al., 1999; Schroeder et al., 1990). We found that the effects of quinpirole were mimicked by the PKC activator phorbol 12-myristate 13-acetate (PMA, 10 μM, normalized ΔG/R: 0.55 ± 0.03, n = 6; Figures 1E and 1G), but not by the PKA activator forskolin (50 μM, normalized ΔG/R: 1.04 ± 0.06, n = 2). Further, quinpirole-mediated effects on AIS Ca^{2+} were blocked by the PKC inhibitor GF109203X (1 μM) and the PKC inhibitor peptide $PKC_{19–31}$ (5 μM, in pipette) (Figures 1F and 1G; quin. + GF: 0.95 ± 0.02, n = 6; quin. + $PKC_{19–31}$: 0.98 ± 0.02, n = 3; PMA + $PKC_{19–31}$: 0.92 ± 0.02, n = 6; $p < 0.0001$ for each blocker versus quinpirole). Thus, AIS Ca^{2+} channels were modulated by dopamine signaling via D_3R-dependent activation of PKC.

D_3R-PKC Pathway Is Specific for AIS T-Type Ca^{2+} Channels

Pharmacological results suggest that D_3R-PKC pathway modulates T-type channels in the AIS. To confirm these results, we isolated T-currents (I_T) in voltage-clamp using a Cs^+-based internal solution and an external solution containing TTX, Cs^+, NBQX, strychnine, and SR95531. I_T was isolated from other Ca^{2+} channel currents with voltage steps from −100 to −60 mV, and whole-cell I_T was recorded while simultaneously imaging Ca^{2+} transients in the AIS and a neighboring dendritic branch (Figures 2A and 2B). This voltage step protocol evoked −493 ± 46 pA I_T in cartwheel cells (n = 28). Mibefradil blocked I_T by 90.7% ± 1.1% and AIS and dendritic Ca^{2+} transients by 88.2% ± 1.1% and 86.5% ± 5.5%, respectively (n = 4 cells) (10 μM, required for block from −100 mV; McDonough and Bean, 1998). Further, the $Ca_V3.2$ selective antagonist ascorbate (300 μM; Nelson et al., 2007) decreased AIS and dendritic Ca^{2+} transients, as well as I_T (Figures 2C and 2D; AIS normalized ΔG/R: 0.62 ± 0.06, dendrite: 0.75 ± 0.06; I_T: 0.57 ± 0.07, n = 4). These data are consistent with previous results with 50 μM Ni^{2+} application (Bender and Trussell, 2009) and suggest that cartwheel cells express $Ca_V3.2$ channels in the AIS and dendrite.

When the D_3R-PKC pathway was activated with quinpirole or PMA, Ca^{2+} transients in the AIS were reduced, but surprisingly, Ca^{2+} transients in the dendrites were not (Figures 2B and 2D; e.g., quinpirole AIS normalized ΔG/R: 0.62 ± 0.06, dendrite: 0.96 ± 0.05, n = 5, $p < 0.02$, paired t test). I_T was also unchanged (Figure 2C; quinpirole normalized I_T: 1.03 ± 0.01, n = 5, PMA: 1.05 ± 0.03, n = 8; $p > 0.5$ versus control for each), probably because the contribution of dendritic T-type channels dominated the whole-cell I_T; however, it was possible that the reduction in I_T due to AIS Ca^{2+} channel block was small compared to the variance in I_T observed over the course of an experiment. To test whether acute blockade of AIS Ca^{2+} channels could affect whole cell I_T, we selectively blocked AIS Ca^{2+} channels with local Ni^{2+} iontophoresis (Bender and Trussell, 2009). In these experiments, control and Ni^{2+}-paired currents were interleaved, eliminating time-dependent changes to I_T. Local Ni^{2+} application reduced AIS Ca^{2+} transients more effectively than the D_3R-PKC pathway (Figure 2D; normalized ΔG/R: 0.41 ± 0.08, n = 3, $p < 0.01$ versus quin. and PMA), but still whole-cell I_T was unaffected (Figure 2C; normalized I_T: 1.00 ± 0.002, $p > 0.3$ versus quinpirole or PMA). Similar results were obtained when the iontophoretic pipette was moved to an isolated dendritic branch (data not shown), confirming that local block of a small fraction of a cell's T-type channels cannot be resolved in whole-cell current recorded in the soma. Thus, dopamine regulates T-type Ca^{2+} channels localized to the AIS, not the dendrite.

Dopamine Activation Reduces Neuronal Output

T-type channels contribute to neuronal excitation and are activated at relatively negative membrane potentials. As a result,

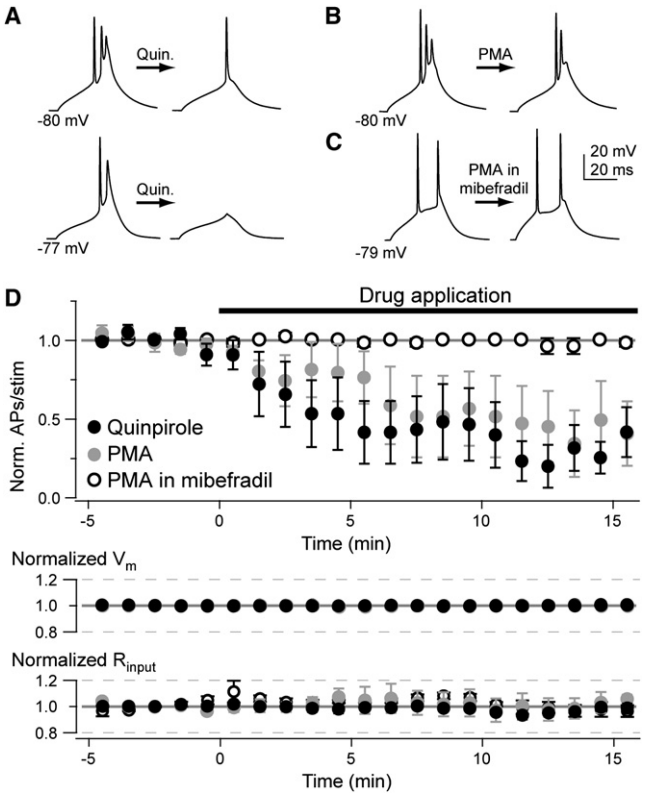

Figure 3. Dopamine Reduces Action Potential Output

(A) AP bursts evoked with somatic current injection during a baseline period (left) and after quinpirole application (right). Current injection was not altered over the course of an experiment.

(B) Same as (A), but with PMA.

(C) Same as (B), but in the presence of mibefradil throughout the recording.

(D) Time course of AP inhibition by quinpirole and PMA. Data were normalized to the baseline number of APs evoked per stimulus. Bars are SEM.

See also Figure S1.

partial blockade of T-type channels with local mibefradil or Ni^{2+} application results in elevation of AP thresholds. Indeed, APs evoked by a given synaptic input are either delayed or never initiated under these conditions (Bender and Trussell, 2009). Since the D_3R-PKC pathway reduces AIS Ca^{2+} influx, its activation should have similar effects on neuronal output. To test this, we evoked APs with 30 ms current pulses just suprathreshold for bursts of 2–3 APs. Cartwheel cells reliably evoked bursts throughout whole-cell recordings (control recordings: 2.6 ± 0.3 APs/stim, 0–5 min; 2.5 ± 0.4 APs/stim, 15–20 min, n = 5), but when the D_3R-PKC pathway was activated with either quinpirole or PMA, the number of APs evoked per stimulus was reduced by at least 50% (Figure 3; PMA: normalized APs/stim: 0.50 ± 0.18, n = 5; quin.: 0.35 ± 0.17, n = 5, $p < 0.02$ versus control for both).

These effects were not due to changes in intrinsic membrane properties—resting membrane potential and input resistance were unaffected by PMA or quinpirole (Figure 3; e.g., baseline V_m: −80.1 ± 0.6 mV, PMA: −80.0 ± 0.6, p = 0.6; baseline R_{in}: 55.7 ± 8.3 MΩ, PMA: 54.1 ± 7.5, p = 0.36, paired t test). Rather, the reduced excitability was mediated by inhibition of T-type Ca^{2+} channels. When T-type channels were blocked with mibefradil (3 μM), cartwheel cells did not fire characteristic AP bursts (Kim and Trussell, 2007). When the stimulus intensity was then increased, the AIS could be depolarized enough to evoke 2 APs with a 30 ms current injection (Figure 3C; stim. intensity: PMA: 181 ± 21 pA; PMA + mibefradil: 327 ± 38 pA). Under these conditions, PMA did not affect AP output (normalized APs/stim: 0.92 ± 0.07, n = 4, p = 0.86 versus control), indicating that PMA reduced AP initiation through its actions on T-type channels.

To quantify the elevation of spike threshold by the D_3R-PKC pathway, we increased the stimulation intensity by 20 pA to ensure that the first AP in a burst would always be present, even in PMA or quinpirole. Relative to control experiments, AP threshold, as detected in phase plane plots, depolarized by 1.8 mV in quinpirole and by 1.5 mV in PMA (see Figure S1 available online; $p < 0.05$ for both). PMA did not affect threshold after blockade of T-type channels with mibefradil (relative depolarization: 0.2 ± 0.4 mV, $p > 0.7$ versus control), confirming that these effects were mediated by changes to T-type channel activity.

D_3R-PKC Pathway Does Not Affect Na^+ or K^+ Channels

These results indicate that AIS T-type channels are modulated by the D_3R-PKC pathway; however, they do not exclude actions on other AIS ion channels. For example, dopaminergic suppression of Na^+ channel function might have led to reduced activation of voltage-gated Ca^{2+} channels in the AIS. Indeed, dopaminergic signaling is reported to alter Na^+ channel activity, although it is unclear if this modulation extends to AIS Na^+ channels (Cantrell and Catterall, 2001; Dai et al., 2009; Maurice et al., 2004). Therefore, we determined whether quinpirole altered AIS Na^+ channel activity by imaging Na^+ with SBFI (1 mM). In these experiments, AIS Ca^{2+} channels were blocked with 100 μM Ni^{2+} to avoid indirect effects of Ca^{2+} channel modulation on Na^+ influx. In many neurons, Na^+ channel subtype expression varies with distance from the axon hillock. Typically, $Na_V1.1$ or 1.2 channels are expressed in the proximal AIS, whereas $Na_V1.6$ channels are more distal (Hu et al., 2009; Lorincz and Nusser, 2008). As these channels may be subject to different regulatory pathways, we imaged AP train-evoked Na^+ transients at two locations (proximal: 9.7 ± 1.4 μm from the hillock; distal: 24.2 ± 2.2 μm, n = 5). Na^+ transients from individual APs were clearly resolved with SBFI, and were not altered by 1 μM quinpirole (Figures 4A and 4C; proximal normalized $\Delta F/F_0$: 1.01 ± 0.04, distal: 1.02 ± 0.02, n = 5, $p > 0.5$ for each location, one sample t test).

To ensure that our imaging system could detect changes in Na^+ influx that might underlie D_3R-PKC pathway-mediated reductions in neuronal output, we first mimicked the effects of quinpirole and PMA by directly blocking Na^+ channels with tetrodotoxin (TTX). We found that partial block of Na^+ channels with 1 nM TTX was sufficient to reduce AP output to 47.1% ± 12.8% of baseline conditions (Figure S2; n = 7, $p > 0.7$ versus either quinpirole or PMA). Then, we again imaged Na^+ transients in the proximal and distal AIS with SBFI. In contrast to quinpirole, 1 nM TTX reduced AP-evoked Na^+ transients in both regions (Figures 4B and 4C; proximal normalized $\Delta F/F_0$: 0.76 ± 0.04, distal: 0.78 ± 0.03, n = 6, $p < 0.01$ for both, one-sample t test). This reduction in SBFI signal was comparable to the block of

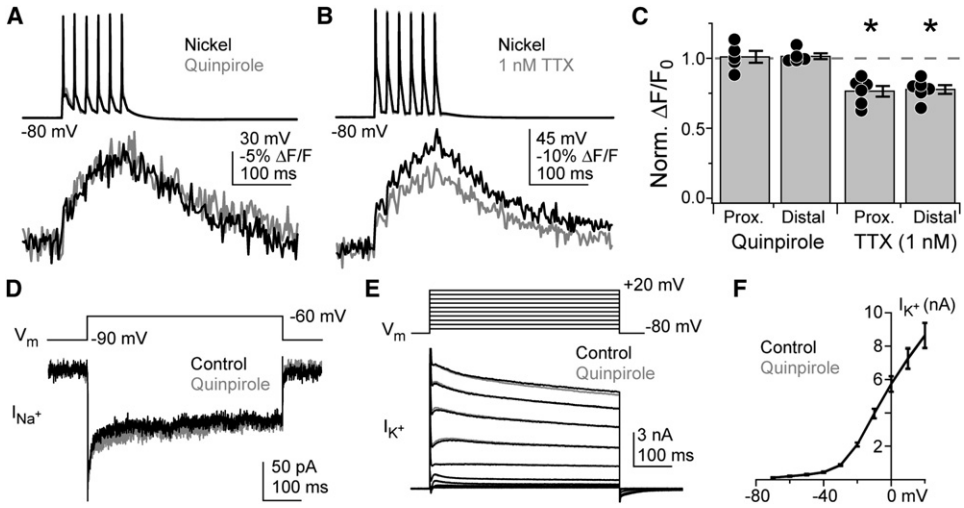

Figure 4. D_3R Signaling Does Not Affect Na^+ or K^+

(A) AP train-evoked Na^+ influx in the AIS, imaged with SBFI, before (black) and after 1 μM quinpirole (gray). Na^+ transients were computed as the change in SBFI fluorescence over baseline.

(B) AP train-evoked Na^+ influx in the AIS before (black) and after 1 nM TTX (gray).

(C) Summary of pharmacological effects on AIS Na^+. Values normalized to baseline $\Delta F/F_0$ amplitudes. Dots are single cells. Error bars are SEM. Asterisk: $p < 0.01$.

(D) Persistent Na^+ currents before (black) and after quinpirole (gray).

(E) K^+ currents before (black) and after quinpirole (gray).

(F) K^+ current versus step voltage. Black: baseline. Grey: quinpirole. Data from each condition superimpose. Bars are SEM.

See also Figure S2.

Na^+ currents observed by voltage clamping $Na_V1.1$, 1.2 and 1.6 channels in heterologous expression systems (Rosker et al., 2007), and indicate that quinpirole had no effect on AIS Na^+ influx.

While transient Na^+ currents cannot be clamped well in whole-cell recordings from dendritic neurons, subthreshold, persistent Na^+ currents can. Both persistent and transient Na^+ currents may originate from the same Na^+ channel source in the AIS (Astman et al., 2006; Fleidervish et al., 2010; Taddese and Bean, 2002). Therefore, whole-cell persistent Na^+ currents provide a second, independent measure of whether quinpirole affects AIS Na^+ channels. TTX-sensitive currents were isolated with voltage steps from −90 to −60 mV in the presence of K^+ channel, Ca^{2+} channel, and ionotropic blockers (Figure 4D; see Experimental Procedures). Consistent with results obtained with SBFI, quinpirole did not alter persistent Na^+ currents (normalized current: 0.99 ± 0.01, n = 6; $p > 0.4$, one-sample t test).

Dopaminergic signaling did not alter V_m or R_{in} in current clamp recordings (Figure 3). This suggests that cartwheel cells lack dopamine-sensitive inward-rectifying K^+ conductances; however, it was still unclear whether dopamine affected other K^+ conductances. To address this, we examined K^+ currents with voltage steps from −80 to +20 mV (10 mV increments), activating K^+ conductances through the full AP voltage range (Figures 4E and 4F). As with Na^+ currents, quinpirole had no effect (e.g., normalized current at −40 mV: 1.03 ± 0.06; at 0 mV: 1.00 ± 0.01; n = 8, $p > 0.9$, repeated-measures ANOVA). Thus, the D_3R-PKC pathway selectively modulates AIS Ca^{2+} channels without affecting AIS Na^+ channels, persistent Na^+ currents, or K^+ currents.

Dopamine Signaling in the DCN

While results described above show that dopamine can alter the output of cartwheel cells, it is unclear whether dopaminergic signaling occurs in the DCN, and if so, whether endogenous dopamine could alter AIS Ca^{2+} channels. To examine these questions, we first determined whether axons capable of dopamine release were present in the DCN. Coronal sections were obtained from mice expressing GFP in all neurons expressing the dopamine synthetic enzyme tyrosine hyroxylase (TH). Consistent with previous reports (Klepper and Herbert, 1991), TH^+ axons were most dense in the fusiform and deep layers, with comparably less innervation in the molecular layer (Figure 5B). This localization could position TH^+ fibers close to cartwheel cell initial segments, since cartwheel somata are often located near the molecular/fusiform cell layer border (Figure 5A). To determine whether TH^+ fibers appose cartwheel axons, we made acute slices from TH-GFP animals and filled cartwheel cells with Alexa 594. GFP and Alexa 594 were visualized simultaneously with two-photon microscopy (excitation wavelength: 880 nm). TH^+ fibers often passed near cartwheel cell initial segments but did not overlap in 10 of 11 cells (Figures 5C and 5D; shortest distance between process centers: 2.6 ± 0.6 μm, range: 0.25–6.52 μm). Given their proximity to the cartwheel AIS, these fibers are a potential source of dopamine.

We next used fast-scan cyclic voltammetry to assess the release of monoamines from the TH^+ fibers in the DCN following stimulation (Heien et al., 2004). A carbon fiber recording electrode was placed serially in the center of the molecular, fusiform, and deep layers, parallel to layer borders. Release was evoked using a monopolar glass electrode placed in the same layer,

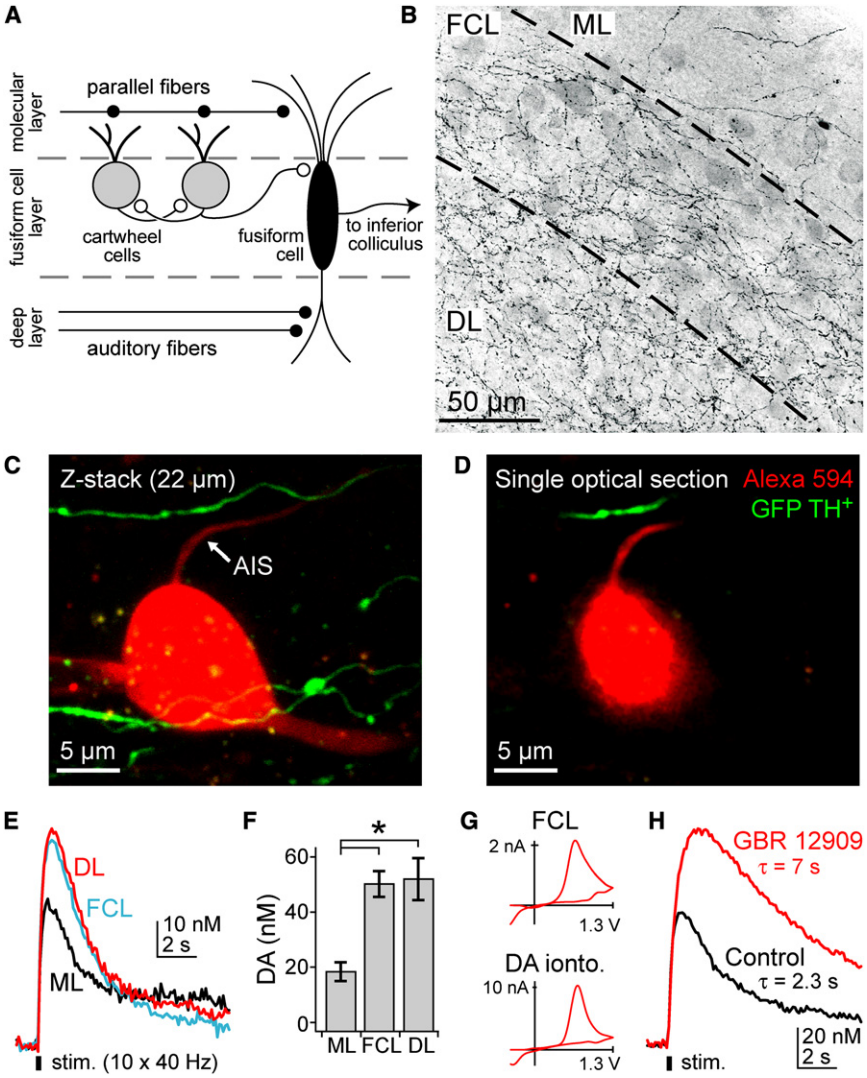

Figure 5. Monoamine Anatomy and Release in the DCN

(A) Schematic DCN circuit. Excitatory synapses are represented by filled circles, inhibitory synapses by open circles. Cartwheel cell somata are typically located near molecular/fusiform cell layer border.

(B) TH^+ axonal fibers in the DCN. Image is a z stack of a 50 µm confocal series. Grayscale inverted for clarity. Dashed lines denote layer borders. ML: molecular layer, FCL: fusiform cell layer, DL: deep layer.

(C) Z stack of cartwheel cell filled with Alexa 594 in a slice from a TH-GFP animal. Recording pipette exits cell on left. GFP-TH^+ axonal fibers are in green, cartwheel cell is filled with Alexa 594 (red).

(D) Single optical section of closest apposition of TH^+ fiber and cartwheel cell axon.

(E) Fast-scan cyclic voltammetric recordings versus time in DCN layers in response to local electrical stimulation in the same layer. Data are single traces all from one slice. Onset and offset of stimulation are indicated by the black bar. Layer abbreviations are as in (B).

(F) Summary of peak dopamine amplitudes in cochlear nucleus layers. Bars are SEM. Asterisk: $p < 0.001$. $n = 12$ slices. Layer abbreviations are as in (B).

(G) Top: representative voltammagram recorded in the fusiform layer. Bottom: voltammagram in response to exogenous dopamine delivered via iontophoresis.

(H) Effect of GBR 12909 on voltammetric recordings in the fusiform layer. Data are single traces.

with trains of 10 stimuli delivered at 40 Hz. Voltammograms recorded in the fusiform cell layer following stimulation were similar in profile to those of exogenous dopamine applied via iontophoresis (Figure 5G). Voltammetric transients were largest in the fusiform and deep layers of the DCN and relatively small in the molecular layer (Figures 5E and 5F). When reuptake was blocked with the specific dopamine transport blocker GBR 12909 (300 nM), voltammetric current increased to 158% ± 15% of baseline (Figure 5H; $n = 12$, $p < 0.01$, paired t test) and their decay slowed by 202% ± 29% ($p < 0.01$, paired t test; baseline τ: 1.7 ± 0.2 s, range: 0.8–2.7 s, $n = 12$). These effects were comparable to those observed in the striatum (Chen and Rice, 2001) and they indicate that dopamine is released from TH^+ fibers in the DCN.

To determine if this endogenous dopamine was sufficient to alter AIS Ca^{2+}, we assayed AP-evoked AIS Ca^{2+} transients before and after local stimulation of dopaminergic fibers. In these experiments, extracellular Ca^{2+} was maintained at 2.4 mM to match voltammetry experiments, and Ca^{2+} was imaged with Fluo-4FF to prevent dye saturation. Ionotropic, $GABA_B$, and mGluR transmission was blocked throughout. Release was evoked using the same stimulation train as in voltammetry experiments (see Experimental Procedures). Stimulating electrodes were placed within 30 µm of visualized cartwheel cell axons, but unfortunately we had no positive control to know whether this placement recruited TH^+ fibers that were in close proximity to the AIS of the recorded cell. As a result, our findings were mixed: AIS Ca^{2+} transients were decreased following stimulation in two cells, but in six others, no change was observed (Figure 6A).

If this experiment was limited by our ability to place the stimulating electrode in the proper position to recruit TH^+ fibers, then the success rate should improve by increasing the effective area of dopaminergic signaling. Therefore, we attenuated monamine reuptake with 300 nM cocaine. In cocaine, AIS Ca^{2+} transients were decreased in 4/7 cells. These effects were not observed in any of 8 cells in the presence of 200 nM sulpiride and 300 nM cocaine (Figures 6B–6D; $p < 0.02$, cocaine versus cocaine + sulpiride), indicating that changes in AIS Ca^{2+} were indeed due to dopaminergic signaling.

Because of the uncertainty of evoking release with local electrical stimulation, we did not test whether AP output was altered.

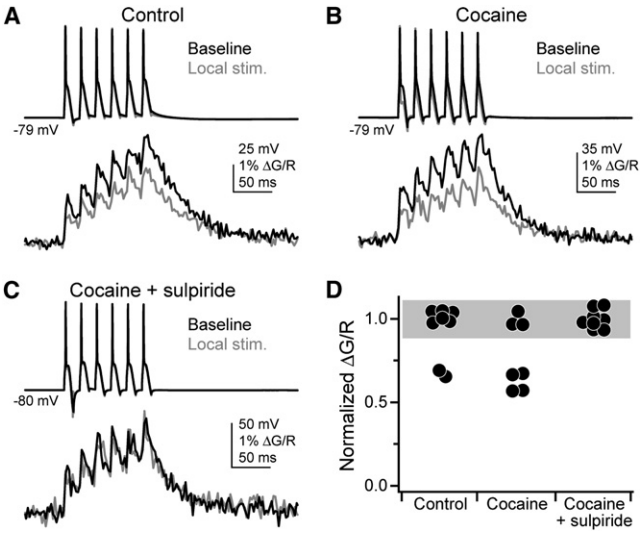

Figure 6. Electrical Stimulation of Dopaminergic Fibers Affects AIS Ca^{2+}

(A) AP train-evoked (top) Ca^{2+} transients (bottom) in the AIS, imaged with Fluo-4FF. Ca^{2+} transients were imaged before (black) and after (gray) dopamine release evoked with local electrical stimulation.

(B) Same as (A), but with 300 nM cocaine present throughout experiment.

(C) Same as (A), but with 300 nM cocaine and 200 nM sulpiride present throughout experiment.

(D) Summary of endogenous dopaminergic fiber stimulation experiments. Values normalized to baseline ΔG/R amplitudes. Dots are single cells. Grey bar represents 2× standard deviation of the cocaine + sulpiride condition, centered on its mean. Any decrements in Ca^{2+} transients below this bar were considered successes.

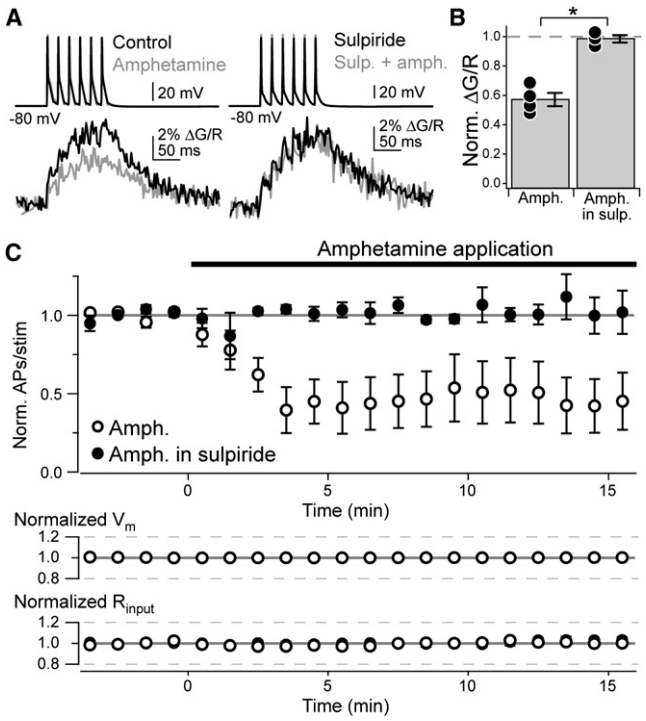

Figure 7. Amphetamine Reduces AIS Ca^{2+} and Spike Output

(A) AP train-evoked Ca^{2+} influx in the AIS, imaged with Fluo-5F. Colors correspond to drug conditions to right of AP trains.

(B) Summary of amphetamine effects on AIS Ca^{2+}. Dots are single cells. Bars are SEM. Asterisk: $p < 0.05$.

(C) Time course of AP inhibition by amphetamine. When required, sulpiride was present throughout the recording. Data normalized to baseline number of APs evoked per stimulus. Bars are SEM.

See also Figure S1.

Instead, we utilized a pharmacological approach and evoked dopamine release by reversing monoamine transporters with amphetamine (10 μM). In contrast to local electrical stimulation, amphetamine consistently decreased AIS Ca^{2+} transients (Figures 7A and 7B; normalized ΔG/R: 0.57 ± 0.05, n = 4). Amphetamine effects were blocked by sulpiride (normalized ΔG/R: 0.99 ± 0.03, n = 3, $p < 0.001$, unpaired t test). Similar to results with quinpirole and PMA, amphetamine reduced the number of APs evoked by 30 ms somatic current pulses (Figure 7C; amphetamine: normalized APs/stim: 0.42 ± 0.15, n = 6; amphetamine in sulpiride: 1.01 ± 0.03, n = 5, $p < 0.01$) and raised AP threshold 1.7 ± 0.4 mV (n = 6, $p < 0.02$ versus amphetamine in sulpiride; Figure S1). Thus, these results establish that dopamine is released from TH^+ fibers in the DCN and can act on cartwheel cell D_3R to alter AIS Ca^{2+} and alter neuronal output.

DISCUSSION

Our results describe a novel mechanism for inhibition of AP initiation by selective dopaminergic modulation of Ca^{2+} channels in the AIS. Dopamine decreased Ca^{2+} influx through AIS T-type channels without altering intrinsic membrane properties, allowing us to isolate the effects of AIS Ca^{2+} modulation on AP output. We found that lowered AIS Ca^{2+} current reduced the rate of local membrane depolarization, which in turn reduced activation rates of local Na^+ channels (Bender and Trussell, 2009), raising AP threshold and thereby reducing AP output.

Several lines of evidence suggest that dopamine-mediated reductions in AIS Ca^{2+} were the result of decreased Ca^{2+} influx through T-type Ca^{2+} channels. AIS Ca^{2+} transients were reduced by D_3R-PKC pathway activation in current clamp (Figure 1), but also in voltage clamp when T-type currents were isolated (Figure 2). This argues against the possibility that dopamine altered membrane potential in the AIS, which then indirectly altered local Ca^{2+} influx. Another possibility is that, since activation of AIS Ca^{2+} and Na^+ channels mutually support regenerative responses (Bender and Trussell, 2009), reductions in local Na^+ influx could in turn reduce Ca^{2+} influx; however, neither AP-evoked Na^+ transients imaged in the AIS or persistent Na^+ currents were affected by quinpirole (Figure 4). Thus, dopamine receptor activation directly modulates AIS T-type channels.

While at this time AIS Ca^{2+} channels have been most thoroughly described in cartwheel cells, Ni^{2+}-sensitive AIS Ca^{2+} transients have been observed in a variety of cell types (Bender and Trussell, 2009), raising the possibility that AIS Ca^{2+} channel modulation is a common mechanism for control of neuronal excitability. Indeed, dopamine reduces neuronal excitability, assessed via whole-cell somatic current injection, in a variety of cell

types, including prefrontal cortex and hippocampal pyramidal cells (Gulledge and Jaffe, 1998; Stanzione et al., 1984; Tseng and O'Donnell, 2004), avian basal ganglia spiny neurons (Ding and Perkel, 2002), and striatal interneurons and medium spiny neurons (Hernandez-Lopez et al., 2000; Maurice et al., 2004). Direct tests will be needed to determine whether alterations to AIS Ca^{2+} influx contribute to reduced excitability in these cells types.

Axon Initial Segment Specificity

Some reports show that T-type Ca^{2+} channels can be downregulated by both D_2R family agonists and PKC, either by reducing open probability or by hyperpolarizing inactivation curves (Lledo et al., 1992; Marchetti et al., 1986), but others show that T currents are not regulated (Chemin et al., 2006; Perez-Reyes, 2003). This disparity suggests that channel regulation depends on a specific set of conditions, fulfilled only when all components are present. We observed a similar mix of results in cartwheel cells: D_3R activation reduced Ca^{2+} influx through axonal, but not dendritic, T-type channels. This specificity suggests that either key components of the D_3R-PKC pathway are localized to the AIS or that T-type channels localized to the AIS are uniquely sensitive to neuromodulation. Of the three T-channel subtypes, the ascorbate and Ni^{2+}-sensitive $Ca_V3.2$ subtype is the most common neuromodulatory target, due to the presence of unique phosphorylation sites found in the intracellular loop between transmembrane domains II and III (Chemin et al., 2006; Lambert et al., 2006). Therefore, we tested if $Ca_V3.2$ channels were exclusively localized to the AIS, but we found that both AIS and dendritic I_T-evoked Ca^{2+} transients were blocked by $Ca_V3.2$-selective antagonists (Figure 2). Thus, selective initial segment modulation is likely not due to the differential localization of T-type isoforms, though we cannot rule out the possibility that the AIS contains a unique splice variant of the $Ca_V3.2$ subtype (Chemin et al., 2006). Most likely, specificity is conferred by upstream components of the D_3R-PKC pathway, or through co-localization of D_3R, PKC, and T-type channels mediated by the cytoskeleton protein ankyrin G, which is restricted to the AIS (Kordeli et al., 1995; Rasband, 2010).

PKC-dependent reductions in AP output occurred within minutes of agonist application (Figures 3 and 7). While protein kinases can translocate upon activation (Zhao et al., 2006), this time scale limits the distance PKC could move before acting on AIS T-type channels. PKA has been shown to translocate from dendritic shaft to spine within seconds of PKA activation (Zhong et al., 2009), but longer distances (e.g., from nucleus to plasma membrane in HEK293 cells, ~5 μm) require >30 min (O'Flaherty et al., 2001). Therefore, we hypothesize that PKC is activated by D_3Rs and acts on Ca^{2+} channels within a small domain, with both D_3Rs and PKC localized to the AIS.

PKC comprises a family of protein kinases, some of which cluster with remarkable subcellular precision. In the AIS, PMA-induced reductions in Ca^{2+} influx were blocked by GF 109203X (Figure 1), a high-affinity inhibitor of classical, Ca^{2+}-dependent PKC isoforms, including PKC-α, PKC-β, PKC-γ, and PKC-ε (Toullec et al., 1991). Of these, D_3R agonists have been shown to activate PKC-γ, inducing a translocation from the cytosol to the cell membrane (Glaser et al., 2003). Consistent with these results, PKC-γ is localized to the AIS in cerebellar Purkinje neurons (Cardell et al., 1998), which share considerable genetic, electrophysiological, and morphological homology with cartwheel cells (Berrebi et al., 1990), and PKC-γ mRNA is highly expressed in both Purkinje cells and cartwheel cells (Lein et al., 2007). Thus, PKC-γ expressed in the AIS may mediate dopaminergic regulation of AIS Ca^{2+}.

Impact of AIS Ca^{2+} Channel Modulation on AP Initiation

Na^+ channel subtypes are differentially compartmentalized in the AIS, with $Na_V1.1/1.2$ channels localized proximal and $Na_V1.6$ channels localized distal to the soma (Hu et al., 2009; Lorincz and Nusser, 2008; Osorio et al., 2005). Because $Na_V1.6$ channels have a low activation threshold, APs initiate in the distal AIS (Hu et al., 2009; Kole and Stuart, 2008; Palmer and Stuart, 2006; Royeck et al., 2008). Interestingly, $Na_V1.6$ channels lack a key serine residue, S573, required for phosphorylation-mediated modulation (Cantrell and Catterall, 2001; Maurice et al., 2001), suggesting that the Na^+ channels responsible for AP initiation may be insensitive to protein kinase-based modulation. Na^+ imaging supports this idea (Figure 4), indicating that quinpirole did not alter Na^+ influx in the cartwheel cell AIS.

We found that the D_3R-PKC pathway acted not on AIS Na^+ channels but on AIS T-type Ca^{2+} channels. This may be an advantageous mechanism for regulating neuronal output. For example, if $Na_V1.6$ channels were downregulated, not only would AP initiation probability be reduced, but the rising phase of the AP would also be altered significantly. This would likely alter neurotransmitter release at downstream axonal boutons, which is dependent on the waveform of the incoming AP (Kole et al., 2007). Since AIS Ca^{2+} channels are not directly responsible for the rising or falling phases of an AP, modification of AIS Ca^{2+} channels could determine whether or not a given stimulus results in AP initiation while leaving the AP waveform largely unaffected. Further, T-type Ca^{2+} channels are strongly linked to bursting activity in many neurons, especially when bursts are evoked from hyperpolarized potentials (Lisman, 1997). Indeed, quinpirole has been shown to reduce bursting behavior in hippocampal pyramidal cells (Stanzione et al., 1984), though it remains unclear whether these changes were mediated by AIS Ca^{2+} channel modulation. In cartwheel cells, bursts at the onset of a stimulus are preferentially evoked from more hyperpolarized potentials (Kim and Trussell, 2007) and, as such, may serve to encode the recent membrane potential history of a cartwheel cell to postsynaptic targets (Uebachs et al., 2006). Alterations in AIS Ca^{2+} therefore may act as a switch, controlling how synaptic inputs are encoded as APs.

Ca^{2+} activates many neuronal signaling pathways, from transmitter release to gene regulation. Therefore, it is likely that AIS Ca^{2+} channels contribute not just to local membrane depolarization, but also to Ca^{2+}-dependent signaling in the AIS. The overall length and location of the AIS relative to the soma dramatically influences neuronal excitability, and this location is fine tuned to the computational tasks of a given neuron (Kress et al., 2010; Kuba et al., 2006). Recent results in both chick auditory brainstem and cultured hippocampal neurons suggest that the AIS position and size are dynamically regulated by recent experience (Grubb and Burrone, 2010; Kuba et al., 2010). This

regulation appears to be homeostatic: increased activity promotes a distal movement of the AIS from the soma, consequently lowering neuronal excitability (Grubb and Burrone, 2010), whereas sensory deprivation promotes an increase in the length of the AIS, increasing overall Na^+ receptor number and thus enhancing neuronal excitability (Kuba et al., 2010). While it has yet to be tested in vivo, these plastic changes in AIS position were mediated by low-threshold Ca^{2+} channel activity in cultured neurons (Grubb and Burrone, 2010). These results, combined with those implicating Ca^{2+}-dependent processes in the dismantling of the AIS after ischemic insult (Schafer et al., 2009), strongly suggest that AIS Ca^{2+} channels play an important role in the maintenance and plasticity of the initial segment.

Implications for Auditory Processing

Neuromodulators play a key role in sensory processing, altering neural circuit dynamics to aid in feature extraction (Hurley et al., 2004). While the cellular mechanisms of neuromodulation have been described primarily in higher brain regions, it has become increasingly clear that neuromodulation occurs at even the earliest stages of sensory processing (Hurley et al., 2004; Kothmann et al., 2009; Petzold et al., 2009). Dopaminergic projections from the brainstem to the cochlea have been proposed to have a protective effect on acoustic function (Darrow et al., 2006). Our data suggest that dopaminergic signaling plays a role in processing of auditory signals in the DCN. In this nucleus, direct auditory nerve input is compared with nonauditory modalities that may encode for head orientation and self-generated noise, aiding in sound localization (Oertel and Young, 2004; Shore and Zhou, 2006; Young and Davis, 2001). Synapses conveying nonauditory information exhibit robust synaptic plasticity (Fujino and Oertel, 2003; Tzounopoulos et al., 2004), suggesting that circuits in the DCN can be altered by experience. Catecholaminergic signaling potentially adds another level of experience-dependent modulation to DCN processing. Our results suggest that dopaminergic activity would dramatically alter the output of cartwheel cells, either by reducing overall activity or by selectively lowering burst output. Within a cartwheel cell, AIS dopaminergic signaling could affect dendritic processing, since bursts evoke large dendritic Ca^{2+} transients (Molitor and Manis, 2003; Roberts et al., 2008). Postsynaptic to cartwheel cells, this pathway could alter inhibitory filtering of nonauditory information, which is conveyed by parallel fibers that synapse on both cartwheel and fusiform cells (Figure 5A). Dopamine could serve to alter the balance of excitation that fusiform cells receive from auditory and nonauditory streams, thereby altering DCN output. It will therefore be of great interest to determine the conditions under which dopaminergic signaling is recruited in the cochlear nucleus and the overall effect dopamine signaling has on sound processing.

EXPERIMENTAL PROCEDURES

Electrophysiology

All procedures were in accordance with OHSU IACUC guidelines. Following anesthesia, coronal brainstem slices (210 μm) were made from P16–24 CBA, ICR, or C57 mice. Transgenic animals (BAC TH-GFP and *D3*$^{-/-}$/$^{+/-}$) were genotyped by PCR. No differences were observed across mouse strains, and results were pooled. Cutting solution contained (in mM) 87 mM NaCl, 25 mM $NaHCO_3$, 25 mM glucose, 75 mM sucrose, 2.5 mM KCl, 1.25 mM NaH_2PO_4, 0.5 mM $CaCl_2$, and 7 mM $MgCl_2$; bubbled with 5%CO_2/95%O_2; 4°C. Following cutting, slices were incubated in the same solution for 30 min at 33°C, then at room temperature until recording. Recording solution contained (in mM) 130 NaCl, 3 KCl, 2.4 $CaCl_2$, 1.3 $MgSO_4$, 1.2 KH_2PO_4, 20 $NaHCO_3$, 3 Na-HEPES, 10 glucose; bubbled with 5%CO_2/95%O_2; 32-34°C. To avoid dye saturation, $CaCl_2$ was reduced to 1 mM and $MgSO_4$ was raised to 2.7 mM for all experiments in which AIS Ca^{2+} transients were evoked by AP trains in current clamp and imaged with Fluo-5F. For all other experiments, including AP-evoked AIS Ca^{2+} imaging with Fluo-4FF, 2.4 mM $CaCl_2$ was used. In all recordings, 10 μM NBQX, 0.5 μM strychnine, and 20 μM SR95531 were added to the recording solution to block synaptic activity. When endogenous dopamine sources were stimulated electrically, 50 μM D-AP5, 2 μM CGP-55845, 1 mM MCPG, and 100 μM LY 341495 were also added to the recording solution to block NMDA, $GABA_B$, and mGluR transmission.

Cartwheel cells were visualized with Dodt contrast optics and identified based on their laminar position, dendritic morphology, and ability to fire complex spikes in response to somatic depolarization (Wouterlood and Mugnaini, 1984). For current clamp recordings, patch electrodes (Schott 8250 glass, 3–4 MΩ tip resistance, <10 MΩ series resistance) were filled with a solution containing (in mM) 113 K-Gluconate, 9 HEPES, 4.5 $MgCl_2$, 0.1 EGTA, 14 $Tris_2$-phosphocreatine, 4 Na_2-ATP, 0.3 tris-GTP; ~290 mOsm (pH 7.2–7.25). For Na^+ imaging, 1 mM SBFI was added to the pipette solution. For Ca^{2+} imaging, EGTA was omitted while 250 μM Fluo-5F and 20 μM Alexa 594 were added to the pipette solution. Electrophysiological data were recorded at 20–50 kHz and filtered at 10 kHz using a Multiclamp 700B amplifier (Molecular Devices), and acquired with an ITC-18 interface (Instrutech) and Igor Pro (Wavemetrics). V_m was held < −75 mV with constant current injection. For imaging experiments, AP trains were evoked via somatic depolarization (1–2 nA, 2 ms), followed by hyperpolarizing steps to prevent AP burst generation (2–400 pA, 10 ms). For experiments assaying AP output following D_3R-PKC pathway activation, AP bursts were evoked with 30 ms step depolarizations. Baseline and postdrug measurements of V_m and R_{in} are the average of −5 to 0 and 5 to 15 min following drug application, respectively. V_m was held to within 2% of baseline values, and cells were excluded if R_{in} changed by > ±7.5%. Data were corrected for a measured junction potential of 12 mV.

Two-Photon Imaging

A two-photon imaging system (Prairie Technologies) was used as described previously (Bender and Trussell, 2009). The laser was tuned to 810 and 790 nm for Ca^{2+} and Na^+ imaging, respectively. Epi- and transfluorescence signals were captured through a 60×, 1.0 NA objective and a 1.4 NA oil immersion condenser (Olympus). Fluorescence was split into red and green channels using dichroic mirrors and band-pass filters (epi: 575 DCXR, HQ525/70, HQ607/45; trans: T560LPXR, ET510/80, ET620/60; Chroma). Green fluorescence (Fluo-5F, SBFI) was captured with R9110 or H8224 photomultiplier tubes (PMTs, Hamamatsu). H8224 PMTs have a higher signal-to-noise ratio than R9110 PMTs. This difference is evident in individual examples in Figure 1, which were imaged with either R9110 (e.g., Figures 1E and 1F) or H8224 PMTs (e.g., Figures 1B–1D). All SBFI and Fluo-4FF imaging experiments were performed with H8224 PMTs. Red fluorescence (Alexa 594) was captured with R9110 PMTs. Data were collected in linescan mode (2–2.4 ms/line, including mirror flyback). For Ca^{2+} imaging, data were presented as averages of 20–40 events per site, and expressed as $\Delta(G/R)/(G/R)_{max}*100$, where $(G/R)_{max}$ was the maximal fluorescence in saturating Ca^{2+} (2 mM; Yasuda et al., 2004). For Na^+ imaging, data were presented as averages of 20 events per site, and expressed as $\Delta F/F_0$, where F_0 is the baseline fluorescence 0–200 ms before stimulus onset. Ca^{2+} and Na^+ transient peaks were calculated from the peak of exponential fits to the fluorescence decay following stimulus offset.

Voltage Clamp of Ca^{2+}, Na^+, and K^+ Currents

For Ca^{2+} and Na^+ currents, internal solution contained (in mM) 110 $CsMeSO_3$, 40 HEPES, 1 KCl, 4 NaCl, 4 Mg-ATP, 10 Na-phosphocreatine, 0.4 Na_2-GTP, 0.5 Fluo-5F, 0.02 Alexa 594; ~290 mOsm (pH 7.22), voltages adjusted for

10 mV junction potential. For K^+ currents, internal solution was the same as for current clamp recordings.

T-type Ca^{2+} currents were activated with 100 ms voltage steps from −100 to −60 mV. Leak currents were subtracted using a P/4 protocol with −10 mV steps from −80 mV. Experiments were performed in the presence of 500 nM TTX, 20 μM SR95531, 500 nM strychnine, 10 μM NBQX, 1 mM Cs^+, and 2.4 mM external Ca^{2+}. Local Ni^{2+} iontophoretic block of AIS Ca^{2+} channels was performed as described previously (Bender and Trussell, 2009). Phosphates were omitted from the recording solution for these experiments.

Persistent Na^+ currents were activated with 500 ms voltage steps from −90 to −60, with leak currents subtracted with −7.5 mV steps from −80 mV. Current amplitudes were calculated as the average of the last 100 ms of each step. Experiments were performed in 20 μM SR95531, 500 nM strychnine, 10 μM NBQX, 10 mM TEA, 2 mM 4-AP, 200 μM Cd^{2+}, 3 μM mibefradil, and 1 mM Cs^+.

K^+ currents were activated with 500 ms voltage steps from −80 to 0 mV in 10 mV increments. Current amplitudes were calculated as the average of the last 10 ms of each step. Experiments were performed in 500 nM TTX, 20 μM SR95531, 500 nM strychnine, 10 μM NBQX, and 1 mM Cs^+. Ca^{2+} channels were not blocked to allow for activation of Ca^{2+}-dependent K^+ channels.

Electrochemistry

Glass-encased carbon fiber electrodes (diameter 7 μm, length 30–50 μm) were placed ~100 μm below the slice surface, parallel to the ependyma, in the center of each DCN layer. Electrodes were fabricated as described previously (Ford et al., 2009; Stamford, 1990). Prior to use, the cut electrode tip was placed in isopropanol purified with activated carbon for 10 min. Monoamine release was evoked with a glass stimulating electrode (stimulation: 10× at 40 Hz, 33 μA, 0.5 ms each) placed in the same layer. This stimulus evoked near-maximal dopamine release within each train and mimicked burst activity commonly observed in dopaminergic neurons. Ten Hertz triangular waveforms (−0.4 to +1.3 V versus Ag/AgCl, 400 V/s) were used for voltammetric recording of monoamines. Background-subtracted cyclic voltammogram currents were obtained by subtracting 10 cyclic voltammograms obtained before stimulation from voltammograms obtained after stimulation. After subtraction, two-dimensional voltammetric color plots were used to examine the data. To determine the voltammetrically detected monoamine time course, the current at the peak oxidation was plotted against time. As observed in other brain regions, voltammetric responses showed run down (Rice et al., 1997). Therefore, for laminar profiles, we stimulated only once in each layer. To assess the effects of GBR 12909, we limited run down by stimulating every 5 min. GBR 12909 was added to the bath only after responses stabilized. Due to limitations in maintaining stable whole-cell recordings >1 hr, trains were evoked at higher frequencies (30× at 0.05 Hz) for experiments described in Figure 6. Transmission may have run down during these protocols, but effects of dopaminergic signaling were still observed. Decay kinetics were determined by a single exponential fit from 90% of the peak (~1.5 s post-stimulation) to 10 s post-stimulation. Currents were calibrated against dopamine standards ranging from 0.05 to 1 μM.

Immunohistochemistry

A mouse expressing GFP in TH^+ cells was fixed with 4% paraformaldehyde via transcardial perfusion. Coronal sections (50 μm) containing the DCN were permeabilized with 0.2% Triton-X, blocked with 10% normal donkey serum, and stained with an anti-GFP antibody conjugated to Alexa 488 (1:500, Invitrogen). Sections were subsequently washed, dehydrated and delipidized, then rehydrated and coverslipped with Fluoromount G (Southern Biotechnology Associates). Fluorescence was acquired with a confocal microscope (60× objective, 1.42 NA).

Chemicals

Fluo-5F pentapotassium salt, SBFI tetraammonium salt, and Alexa Fluor 594 hydrazide Na^+ salt were from Invitrogen. SR95531, D-AP5, and NBQX were from Ascent. (−)-quinpirole hydrochloride, PMA, (S)-MCPG, CGP-55845, LY-341495, tetrodotoxin (TTX), and GF 109203X were from Tocris. $PKC_{19–31}$ was from Calbiochem. All others were from Sigma.

Statistics

All data are shown as mean ± standard error (SEM). An ANOVA followed by Fisher's PLSD post hoc test was used unless otherwise noted (significance, $p < 0.05$).

SUPPLEMENTAL INFORMATION

Supplemental Information includes two figures and can be found with this article online at doi:10.1016/j.neuron.2010.09.026.

ACKNOWLEDGMENTS

We are grateful to J. Trapani, J. Deignan, and members of the Trussell and Williams labs for comments, and to J. Williams for reading the manuscript. We thank D. Grandy and J. Williams for knockout and transgenic mice, and to A. Truitt, M. Grandy, K. Suchland, A. Matsui, and N. Quillinan for genotyping expertise. This research was supported by NIH grants K99DC011080 (K.J.B.), K99DA026417 (C.P.F.), and NS028901 (L.O.T.).

Accepted: September 8, 2010
Published: November 3, 2010

REFERENCES

Astman, N., Gutnick, M.J., and Fleidervish, I.A. (2006). Persistent sodium current in layer 5 neocortical neurons is primarily generated in the proximal axon. J. Neurosci. *26*, 3465–3473.

Azouz, R., and Gray, C.M. (2000). Dynamic spike threshold reveals a mechanism for synaptic coincidence detection in cortical neurons in vivo. Proc. Natl. Acad. Sci. USA *97*, 8110–8115.

Bean, B.P. (2007). The action potential in mammalian central neurons. Nat. Rev. Neurosci. *8*, 451–465.

Bender, K.J., and Trussell, L.O. (2009). Axon initial segment Ca^{2+} channels influence action potential generation and timing. Neuron *61*, 259–271.

Berrebi, A.S., Morgan, J.I., and Mugnaini, E. (1990). The Purkinje cell class may extend beyond the cerebellum. J. Neurocytol. *19*, 643–654.

Bouthenet, M.L., Souil, E., Martres, M.P., Sokoloff, P., Giros, B., and Schwartz, J.C. (1991). Localization of dopamine D3 receptor mRNA in the rat brain using in situ hybridization histochemistry: comparison with dopamine D2 receptor mRNA. Brain Res. *564*, 203–219.

Callewaert, G., Eilers, J., and Konnerth, A. (1996). Axonal calcium entry during fast 'sodium' action potentials in rat cerebellar Purkinje neurones. J. Physiol. *495*, 641–647.

Cantrell, A.R., and Catterall, W.A. (2001). Neuromodulation of Na^+ channels: An unexpected form of cellular plasticity. Nat. Rev. Neurosci. *2*, 397–407.

Cardell, M., Landsend, A.S., Eidet, J., Wieloch, T., Blackstad, T.W., and Ottersen, O.P. (1998). High resolution immunogold analysis reveals distinct subcellular compartmentation of protein kinase C gamma and delta in rat Purkinje cells. Neuroscience *82*, 709–725.

Chemin, J., Traboulsie, A., and Lory, P. (2006). Molecular pathways underlying the modulation of T-type calcium channels by neurotransmitters and hormones. Cell Calcium *40*, 121–134.

Chen, B.T., and Rice, M.E. (2001). Novel Ca^{2+} dependence and time course of somatodendritic dopamine release: substantia nigra versus striatum. J. Neurosci. *21*, 7841–7847.

Coombs, J.S., Curtis, D.R., and Eccles, J.C. (1957). The interpretation of spike potentials of motoneurones. J. Physiol. *139*, 198–231.

Dai, Y., Jordan, L.M., and Fedirchuk, B. (2009). Modulation of transient and persistent inward currents by activation of protein kinase C in spinal ventral neurons of the neonatal rat. J. Neurophysiol. *101*, 112–128.

Darrow, K.N., Simons, E.J., Dodds, L., and Liberman, M.C. (2006). Dopaminergic innervation of the mouse inner ear: evidence for a separate cytochemical group of cochlear efferent fibers. J. Comp. Neurol. *498*, 403–414.

Ding, L., and Perkel, D.J. (2002). Dopamine modulates excitability of spiny neurons in the avian basal ganglia. J. Neurosci. *22*, 5210–5218.

Fleidervish, I.A., Lasser-Ross, N., Gutnick, M.J., and Ross, W.N. (2010). Na^+ imaging reveals little difference in action potential-evoked Na^+ influx between axon and soma. Nat. Neurosci. *13*, 852–860.

Ford, C.P., Phillips, P.E., and Williams, J.T. (2009). The time course of dopamine transmission in the ventral tegmental area. J. Neurosci. *29*, 13344–13352.

Fujino, K., and Oertel, D. (2003). Bidirectional synaptic plasticity in the cerebellum-like mammalian dorsal cochlear nucleus. Proc. Natl. Acad. Sci. USA *100*, 265–270.

Glaser, S., Alvaro, D., Roskams, T., Phinizy, J.L., Stoica, G., Francis, H., Ueno, Y., Barbaro, B., Marzioni, M., Mauldin, J., et al. (2003). Dopaminergic inhibition of secretin-stimulated choleresis by increased PKC-gamma expression and decrease of PKA activity. Am. J. Physiol. Gastrointest. Liver Physiol. *284*, G683–G694.

Goldberg, E.M., Clark, B.D., Zagha, E., Nahmani, M., Erisir, A., and Rudy, B. (2008). K^+ channels at the axon initial segment dampen near-threshold excitability of neocortical fast-spiking GABAergic interneurons. Neuron *58*, 387–400.

Grubb, M.S., and Burrone, J. (2010). Activity-dependent relocation of the axon initial segment fine-tunes neuronal excitability. Nature *465*, 1070–1074.

Gulledge, A.T., and Jaffe, D.B. (1998). Dopamine decreases the excitability of layer V pyramidal cells in the rat prefrontal cortex. J. Neurosci. *18*, 9139–9151.

Heien, M.L., Johnson, M.A., and Wightman, R.M. (2004). Resolving neurotransmitters detected by fast-scan cyclic voltammetry. Anal. Chem. *76*, 5697–5704.

Heintz, N. (2004). Gene expression nervous system atlas (GENSAT). Nat. Neurosci. *7*, 483.

Hernandez-Lopez, S., Tkatch, T., Perez-Garci, E., Galarraga, E., Bargas, J., Hamm, H., and Surmeier, D.J. (2000). D2 dopamine receptors in striatal medium spiny neurons reduce L-type Ca^{2+} currents and excitability via a novel PLCβ1-IP3-calcineurin-signaling cascade. J. Neurosci. *20*, 8987–8995.

Hu, W., Tian, C., Li, T., Yang, M., Hou, H., and Shu, Y. (2009). Distinct contributions of Na(v)1.6 and Na(v)1.2 in action potential initiation and backpropagation. Nat. Neurosci. *12*, 996–1002.

Hurley, L.M., Devilbiss, D.M., and Waterhouse, B.D. (2004). A matter of focus: Monoaminergic modulation of stimulus coding in mammalian sensory networks. Curr. Opin. Neurobiol. *14*, 488–495.

Khaliq, Z.M., and Raman, I.M. (2006). Relative contributions of axonal and somatic Na channels to action potential initiation in cerebellar Purkinje neurons. J. Neurosci. *26*, 1935–1944.

Kim, Y., and Trussell, L.O. (2007). Ion channels generating complex spikes in cartwheel cells of the dorsal cochlear nucleus. J. Neurophysiol. *97*, 1705–1725.

Klepper, A., and Herbert, H. (1991). Distribution and origin of noradrenergic and serotonergic fibers in the cochlear nucleus and inferior colliculus of the rat. Brain Res. *557*, 190–201.

Kole, M.H., and Stuart, G.J. (2008). Is action potential threshold lowest in the axon? Nat. Neurosci. *11*, 1253–1255.

Kole, M.H., Letzkus, J.J., and Stuart, G.J. (2007). Axon initial segment Kv1 channels control axonal action potential waveform and synaptic efficacy. Neuron *55*, 633–647.

Kordeli, E., Lambert, S., and Bennett, V. (1995). AnkyrinG. A new ankyrin gene with neural-specific isoforms localized at the axonal initial segment and node of Ranvier. J. Biol. Chem. *270*, 2352–2359.

Kothmann, W.W., Massey, S.C., and O'Brien, J. (2009). Dopamine-stimulated dephosphorylation of connexin 36 mediates AII amacrine cell uncoupling. J. Neurosci. *29*, 14903–14911.

Kress, G.J., and Mennerick, S. (2009). Action potential initiation and propagation: upstream influences on neurotransmission. Neuroscience *158*, 211–222.

Kress, G.J., Dowling, M.J., Meeks, J.P., and Mennerick, S. (2008). High threshold, proximal initiation, and slow conduction velocity of action potentials in dentate granule neuron mossy fibers. J. Neurophysiol. *100*, 281–291.

Kress, G.J., Dowling, M.J., Eisenman, L.N., and Mennerick, S. (2010). Axonal sodium channel distribution shapes the depolarized action potential threshold of dentate granule neurons. Hippocampus *20*, 558–571.

Kuba, H., Ishii, T.M., and Ohmori, H. (2006). Axonal site of spike initiation enhances auditory coincidence detection. Nature *444*, 1069–1072.

Kuba, H., Oichi, Y., and Ohmori, H. (2010). Presynaptic activity regulates Na(+) channel distribution at the axon initial segment. Nature *465*, 1075–1078.

Lambert, R.C., Bessaih, T., and Leresche, N. (2006). Modulation of neuronal T-type calcium channels. CNS Neurol. Disord. Drug Targets *5*, 611–627.

Lee, J.H., Gomora, J.C., Cribbs, L.L., and Perez-Reyes, E. (1999). Nickel block of three cloned T-type calcium channels: low concentrations selectively block alpha1H. Biophys. J. *77*, 3034–3042.

Lein, E.S., Hawrylycz, M.J., Ao, N., Ayres, M., Bensinger, A., Bernard, A., Boe, A.F., Boguski, M.S., Brockway, K.S., Byrnes, E.J., et al. (2007). Genome-wide atlas of gene expression in the adult mouse brain. Nature *445*, 168–176.

Lisman, J.E. (1997). Bursts as a unit of neural information: Making unreliable synapses reliable. Trends Neurosci. *20*, 38–43.

Lledo, P.M., Homburger, V., Bockaert, J., and Vincent, J.D. (1992). Differential G protein-mediated coupling of D2 dopamine receptors to K^+ and Ca^{2+} currents in rat anterior pituitary cells. Neuron *8*, 455–463.

Lorincz, A., and Nusser, Z. (2008). Cell-type-dependent molecular composition of the axon initial segment. J. Neurosci. *28*, 14329–14340.

Lüscher, C., Lipp, P., Lüscher, H.R., and Niggli, E. (1996). Control of action potential propagation by intracellular Ca^{2+} in cultured rat dorsal root ganglion cells. J. Physiol. *490*, 319–324.

Marchetti, C., Carbone, E., and Lux, H.D. (1986). Effects of dopamine and noradrenaline on Ca channels of cultured sensory and sympathetic neurons of chick. Pflugers Arch. *406*, 104–111.

Martina, M., Vida, I., and Jonas, P. (2000). Distal initiation and active propagation of action potentials in interneuron dendrites. Science *287*, 295–300.

Maurice, N., Tkatch, T., Meisler, M., Sprunger, L.K., and Surmeier, D.J. (2001). D1/D5 dopamine receptor activation differentially modulates rapidly inactivating and persistent sodium currents in prefrontal cortex pyramidal neurons. J. Neurosci. *21*, 2268–2277.

Maurice, N., Mercer, J., Chan, C.S., Hernandez-Lopez, S., Held, J., Tkatch, T., and Surmeier, D.J. (2004). D2 dopamine receptor-mediated modulation of voltage-dependent Na^+ channels reduces autonomous activity in striatal cholinergic interneurons. J. Neurosci. *24*, 10289–10301.

McDonough, S.I., and Bean, B.P. (1998). Mibefradil inhibition of T-type calcium channels in cerebellar purkinje neurons. Mol. Pharmacol. *54*, 1080–1087.

Molitor, S.C., and Manis, P.B. (2003). Dendritic Ca^{2+} transients evoked by action potentials in rat dorsal cochlear nucleus pyramidal and cartwheel neurons. J. Neurophysiol. *89*, 2225–2237.

Nelson, M.T., Joksovic, P.M., Su, P., Kang, H.W., Van Deusen, A., Baumgart, J.P., David, L.S., Snutch, T.P., Barrett, P.Q., Lee, J.H., et al. (2007). Molecular mechanisms of subtype-specific inhibition of neuronal T-type calcium channels by ascorbate. J. Neurosci. *27*, 12577–12583.

O'Flaherty, J.T., Chadwell, B.A., Kearns, M.W., Sergeant, S., and Daniel, L.W. (2001). Protein kinases C translocation responses to low concentrations of arachidonic acid. J. Biol. Chem. *276*, 24743–24750.

Oertel, D., and Young, E.D. (2004). What's a cerebellar circuit doing in the auditory system? Trends Neurosci. *27*, 104–110.

Osorio, N., Alcaraz, G., Padilla, F., Couraud, F., Delmas, P., and Crest, M. (2005). Differential targeting and functional specialization of sodium channels in cultured cerebellar granule cells. J. Physiol. *569*, 801–816.

Palmer, L.M., and Stuart, G.J. (2006). Site of action potential initiation in layer 5 pyramidal neurons. J. Neurosci. *26*, 1854–1863.

Perez-Reyes, E. (2003). Molecular physiology of low-voltage-activated t-type calcium channels. Physiol. Rev. *83*, 117–161.

Petzold, G.C., Hagiwara, A., and Murthy, V.N. (2009). Serotonergic modulation of odor input to the mammalian olfactory bulb. Nat. Neurosci. *12*, 784–791.

Rasband, M.N. (2010). The axon initial segment and the maintenance of neuronal polarity. Nat. Rev. Neurosci. *11*, 552–562.

Rice, M.E., Cragg, S.J., and Greenfield, S.A. (1997). Characteristics of electrically evoked somatodendritic dopamine release in substantia nigra and ventral tegmental area in vitro. J. Neurophysiol. *77*, 853–862.

Roberts, M.T., Bender, K.J., and Trussell, L.O. (2008). Fidelity of complex spike-mediated synaptic transmission between inhibitory interneurons. J. Neurosci. *28*, 9440–9450.

Ron, D., Jiang, Z., Yao, L., Vagts, A., Diamond, I., and Gordon, A. (1999). Coordinated movement of RACK1 with activated betaIIPKC. J. Biol. Chem. *274*, 27039–27046.

Rosker, C., Lohberger, B., Hofer, D., Steinecker, B., Quasthoff, S., and Schreibmayer, W. (2007). The TTX metabolite 4,9-anhydro-TTX is a highly specific blocker of the Na(v1.6) voltage-dependent sodium channel. Am. J. Physiol. Cell Physiol. *293*, C783–C789.

Royeck, M., Horstmann, M.T., Remy, S., Reitze, M., Yaari, Y., and Beck, H. (2008). Role of axonal NaV1.6 sodium channels in action potential initiation of CA1 pyramidal neurons. J. Neurophysiol. *100*, 2361–2380.

Schafer, D.P., Jha, S., Liu, F., Akella, T., McCullough, L.D., and Rasband, M.N. (2009). Disruption of the axon initial segment cytoskeleton is a new mechanism for neuronal injury. J. Neurosci. *29*, 13242–13254.

Schiller, J., Helmchen, F., and Sakmann, B. (1995). Spatial profile of dendritic calcium transients evoked by action potentials in rat neocortical pyramidal neurones. J. Physiol. *487*, 583–600.

Schmidt-Hieber, C., Jonas, P., and Bischofberger, J. (2008). Action potential initiation and propagation in hippocampal mossy fibre axons. J. Physiol. *586*, 1849–1857.

Schroeder, J.E., Fischbach, P.S., and McCleskey, E.W. (1990). T-type calcium channels: heterogeneous expression in rat sensory neurons and selective modulation by phorbol esters. J. Neurosci. *10*, 947–951.

Shore, S.E., and Zhou, J. (2006). Somatosensory influence on the cochlear nucleus and beyond. Hear. Res. *216-217*, 90–99.

Shu, Y., Duque, A., Yu, Y., Haider, B., and McCormick, D.A. (2007). Properties of action-potential initiation in neocortical pyramidal cells: evidence from whole cell axon recordings. J. Neurophysiol. *97*, 746–760.

Stamford, J.A. (1990). Fast cyclic voltammetry: measuring transmitter release in 'real time'. J. Neurosci. Methods *34*, 67–72.

Stanzione, P., Calabresi, P., Mercuri, N., and Bernardi, G. (1984). Dopamine modulates CA1 hippocampal neurons by elevating the threshold for spike generation: an in vitro study. Neuroscience *13*, 1105–1116.

Stuart, G., Schiller, J., and Sakmann, B. (1997). Action potential initiation and propagation in rat neocortical pyramidal neurons. J. Physiol. *505*, 617–632.

Taddese, A., and Bean, B.P. (2002). Subthreshold sodium current from rapidly inactivating sodium channels drives spontaneous firing of tuberomammillary neurons. Neuron *33*, 587–600.

Toullec, D., Pianetti, P., Coste, H., Bellevergue, P., Grand-Perret, T., Ajakane, M., Baudet, V., Boissin, P., Boursier, E., Loriolle, F., et al. (1991). The bisindolylmaleimide GF 109203X is a potent and selective inhibitor of protein kinase C. J. Biol. Chem. *266*, 15771–15781.

Tseng, K.Y., and O'Donnell, P. (2004). Dopamine-glutamate interactions controlling prefrontal cortical pyramidal cell excitability involve multiple signaling mechanisms. J. Neurosci. *24*, 5131–5139.

Tzounopoulos, T., Kim, Y., Oertel, D., and Trussell, L.O. (2004). Cell-specific, spike timing-dependent plasticities in the dorsal cochlear nucleus. Nat. Neurosci. *7*, 719–725.

Uebachs, M., Schaub, C., Perez-Reyes, E., and Beck, H. (2006). T-type Ca^{2+} channels encode prior neuronal activity as modulated recovery rates. J. Physiol. *571*, 519–536.

Wouterlood, F.G., and Mugnaini, E. (1984). Cartwheel neurons of the dorsal cochlear nucleus: a Golgi-electron microscopic study in rat. J. Comp. Neurol. *227*, 136–157.

Yasuda, R., Nimchinsky, E.A., Scheuss, V., Pologruto, T.A., Oertner, T.G., Sabatini, B.L., and Svoboda, K. (2004). Imaging calcium concentration dynamics in small neuronal compartments. Sci. STKE *2004*, pl5.

Young, E.D., and Davis, K.A. (2001). Circuitry and function of the dorsal cochlear nucleus. In Integrative Functions in the Mammalian Auditory Pathway, D. Oertel, A.N. Popper, and R.R. Fay, eds. (New York: Springer-Verlag), pp. 160–206.

Zhao, Y., Leal, K., Abi-Farah, C., Martin, K.C., Sossin, W.S., and Klein, M. (2006). Isoform specificity of PKC translocation in living Aplysia sensory neurons and a role for Ca^{2+}-dependent PKC APL I in the induction of intermediate-term facilitation. J. Neurosci. *26*, 8847–8856.

Zhong, H., Sia, G.M., Sato, T.R., Gray, N.W., Mao, T., Khuchua, Z., Huganir, R.L., and Svoboda, K. (2009). Subcellular dynamics of type II PKA in neurons. Neuron *62*, 363–374.